ISSN 0036-0236, Russian Journal of Inorganic Chemistry, 2023, Vol. 68, No. 8, pp. 1065–1076. © Pleiades Publishing, Ltd., 2023.
ISSN 0036-0236, Russian Journal of Inorganic Chemistry, 2023. © Pleiades Publishing, Ltd., 2023.

INORGANIC MATERIALS AND NANOMATERIALS

Electronic, Structural, and Optical Properties of $Fe(CO)_4[X_{12}Y_{12}]$ (X = B or Al, Y = N or P) Complexes: A Computational Investigation

Hedieh Asadzadeh[a], Reza Ghiasi[b, *, **], Mohammad Yousefi[c], and Sahar Baniyaghoob[a]

[a] *Department of Chemistry, Science and Research Branch, Islamic Azad University, Tehran, Iran*

[b] *Department of Chemistry, East Tehran Branch, Islamic Azad University, Tehran, Iran*

[c] *Department of Chemistry, Faculty of Pharmaceutical Chemistry, Tehran Medical Sciences Branch, Islamic Azad University, Tehran, Iran*

**e-mail: rezaghiasi1353@yahoo.com*

***e-mail: reza.ghiasi@iau.ac.ir*

Received February 2, 2023; revised April 28, 2023; accepted May 12, 2023

Abstract—Electronic, structural, and optical properties of $Fe(CO)_4[X_{12}Y_{12}]$ (X = B or Al, Y = N or P) complexes have been illustrated at the mPW1PW91/6-311G(d,p) level of theory. Two possible isomers of the interaction between $[X_{12}Y_{12}]$ nano-cluster and $Fe(CO)_4$ have been considered. In isomer **I**, $Fe(CO)_4$ fragment interacts with common X–Y bond between six-membered rings. In isomer **II**, this fragment interacts with common X–Y bond between six-membered and four-membered of cage. Dipole moment values, polarizability parameters, and non-linear optical properties of these complexes have been investigated. Energy decomposition analysis (EDA) has been employed to explore the interactions between nano-cluster and $Fe(CO)_4$. Charge transfer between $[X_{12}Y_{12}]$ nano-clusters and $Fe(CO)_4$ fragment has been explored with electrophilicity-based charge transfer (ECT). QTAIM computations have been employed for illustration the characterizations of Fe–C, Fe–X, and Fe–Y bonds in the studied complexes. In addition, Laplacian bond orders (LBO) of the Fe–C, Fe–X, and Fe–Y bonds have been calculated. Independent gradient model (IGM) based on promolecular density has been used to evaluate the interaction between $Fe(CO)_4$ and $[X_{12}Y_{12}]$.

Keywords: nano-cage, $Fe(CO)_4$, electrophilicity-based charge transfer (ECT), energy decomposition analysis (EDA), Laplacian bond order (LBO)

DOI: 10.1134/S0036023623600338

INTRODUCTION

$Fe(CO)_4$ organometallic fragment is isolobal with CH_3^+ organic fragment. Structure, bonding and the related compounds of $Fe(CO)_4$ have been reported [1–3]. The interaction of numerous ligands with the $Fe(CO)_4$ fragment has been considered [4–8]. The interesting structures of the metal–π ligand complexes, giving creative attention within organometallic chemistry [9].

Boron cluster chemistry is an attractive subject in inorganic chemistry [10–17]. Various researches have been reported recently to the $[X_nY_n]$ nano-structures (X = Group III elements, Y = Group V elements) [18–33]. These nano-materials indicate noteworthy chemical and physical properties, for instance wide band-gap semiconductors. The XY bond causes $[X_nY_n]$ molecules to show a reactivity pattern different from that of carbon analogue [34]. $[Al_{12}P_{12}]$ and $[B_{12}P_{12}]$ molecules are valuable nano-cages, and they have suitable adsorption ability, large HOMO–LUMO gap, small electron attraction, and exceptional properties [35–41]. Many researches have been reported on adsorption properties of several molecules on the surface of $[X_{12}P_{12}]$ (X = Al and P) nanocages. A DFT investigation was used on the hydrogen atom interaction with boron phosphide nano-cluster [42]. The consequences illustrated a significant role of electron density of adsorbing atoms in hydrogen adsorption on the boron phosphide nano-cage. In other investigation, computational study of the effect of Ni and Pd transition metal functionalized on Interaction of mercaptopyridine with $[B_{12}N_{12}]$ nano-cage has been reported [43].

DFT investigation of doping of the first row transition metals (from Sc to Zn) onto possible adsorption positions of the outside surface of $[B_{12}N_{12}]$ nano-cage has been reported [44].

An experimental investigation about of tetra-carbonyl derivate of C_{60} has been reported by ^{57}Fe Mossbauer spectroscopy and experimental data compared to similar organometallic complexes [45].

In the basis of our researches, interactions $Fe(CO)_4$ and $[X_{12}Y_{12}]$ (X = B or Al, Y = N or P) nano-cages have been not studied. Therefore, we interested to illustration the electronic, structural and optical prop-

Table 1. Energy (E, a.u.), relative energy (ΔE, kcal/mol), dipole moment (Debye, μ), and isotropic (au, α_{iso}) values of the two modes coordination of $Fe(CO)_4$ fragment to $[X_{12}Y_{12}]$ (X = B or Al, Y = N or P) nano-cages

Molecule	E	ΔE	μ	α_{iso}
BN-**I**	−2673.2333	3.80	1.52	234.81
BN-**II**	−2673.2393	0.00	1.92	234.51
AlN-**I**	−5284.4608	4.15	1.17	366.70
AlN-**II**	−5284.4674	0.00	1.64	365.79
BP-**I**	−6112.0961	1.34	2.57	494.37
BP-**II**	−6112.0982	0.00	2.58	496.07
AlP-**I**	−8723.8805	0.70	1.63	685.34
AlP-**II**	−8723.8816	0.00	2.14	687.24

erties of $Fe(CO)_4$ $[X_{12}Y_{12}]$ (X = B or Al, Y = N or P) complexes at the mPW1PW91/6-311G(d,p) level of theory. Two possible isomers of the interaction between $[X_{12}Y_{12}]$ nano-cluster and $Fe(CO)_4$ are considered. Dipole moment values, polarizability parameters and non-linear optical properties of these complexes are investigated.

COMPUTATION DETAILS

The studied molecules were optimized at the mPW1PW91/6-311G(d,p) level of theory using Gaussian software package [46]. The standard 6-311G (d, p) basis set is considered [47, 48]. the parameter hybrid functional with adapted Perdew-Wang exchange and correlation (mPW1PW91) was considered [49]. This functional is suitable for transition metal complexes in compared to B3LYP [50–53]. Identity of the studied molecules as an energy minimum was considered with a vibrational analysis.

The bonding interaction values between the $Fe(CO)_4$ and $[X_{12}Y_{12}]$ (X = B or Al, Y = N or P) nano-cages were analyzed using the energy decomposition analysis (EDA) handled in Multiwfn 3.5 package [54]. In this analysis, the interaction energy (ΔE_{int}) between two fragments can be divided into three major components:

$$\Delta E_{int} = \Delta E_{polar} + \Delta E_{els} + \Delta E_{Ex},$$

where ΔE_{polar} is electron density polarization term (also called as induction term)

$$\Delta E_{polar} = E(\text{SCF last}) - E(\text{SCF 1st}),$$

where E (SCF last) and E (SCF 1st) are the SCF energy at the first and last cycles of SCF process, respectively; ΔE_{els} is electrostatic interaction term, and ΔE_{Ex} is exchange repulsion term. The last two terms may be combined into a single one, which is called the steric-repulsion term ($\Delta E_{steric} = \Delta E_{els} + \Delta E_{Ex}$).

Bond order values are calculated by Laplacian bond order (LBO) method [55]. This method is definition of covalent bond order based on the Laplacian of electron density $\nabla^2\rho$ in fuzzy overlap space. The LBO between atom A and B can be simply written as

$$L_{A,B} = -10 \times \int_{\nabla^2\rho < 0} w_A(r) w_B(r) \nabla^2\rho(r) dr,$$

where w is a smoothly varying weighting function proposed by Becke and represents fuzzy atomic space; hence, w_A and w_B correspond to fuzzy overlap space between A and B.

Quantum theory of atoms in molecules (QTAIM) analysis, Independent Gradient Model (IGM) analysis based on promolecular density [56, 57] and Laplacian bond order (LBO) values were provided by Multiwfn 3.5 package [58, 59].

The total static first hyperpolarizability (β_{tot}) was computed from the following equation:

$$\beta_{tot} = \sqrt{\beta_x^2 + \beta_y^2 + \beta_z^2},$$

where

$$\beta_i = \beta_{iii} + \frac{1}{3}\sum_{i \neq j}(\beta_{ijj} + \beta_{jij} + \beta_{jji}).$$

The Kleinman symmetry show that [60]:

$$\beta_{xyy} = \beta_{yxy} = \beta_{yyx}; \quad \beta_{yyz} = \beta_{yzy} = \beta_{zyy}.$$

Therefore

$$\beta_{tot} = \sqrt{(\beta_{xxx} + \beta_{xyy} + \beta_{xzz})^2 + (\beta_{yyy} + \beta_{yzz} + \beta_{yxx})^2 + (\beta_{zzz}zxx + \beta_{zyy})^2}$$

RESULTS AND DISCUSSION

Energetics Aspects

Two modes coordination of $Fe(CO)_4$ fragment to $[X_{12}Y_{12}]$ (X = B or Al, Y = N or P) nano-cages are presented in Fig. 1. In isomer **I**, $Fe(CO)_4$ fragment interacts with common X–Y bond between six-membered rings. In isomer **II**, this fragment interacts with common X–Y bond between six-membered and four-membered of cage. Energy and relative energy values of the investigated structures are gathered in Table 1. It can be observed, isomer **II** has more stability than isomer **I**. On the other hand, the relative energy values decrease with increasing of atomic numbers of X and Y.

Bond Distances

The Fe–C, Fe–X and Fe–Y bonding distances of the studied complexes are listed in Table 2. These values reveal Fe–X and Fe–Y bonds are longer in isomer

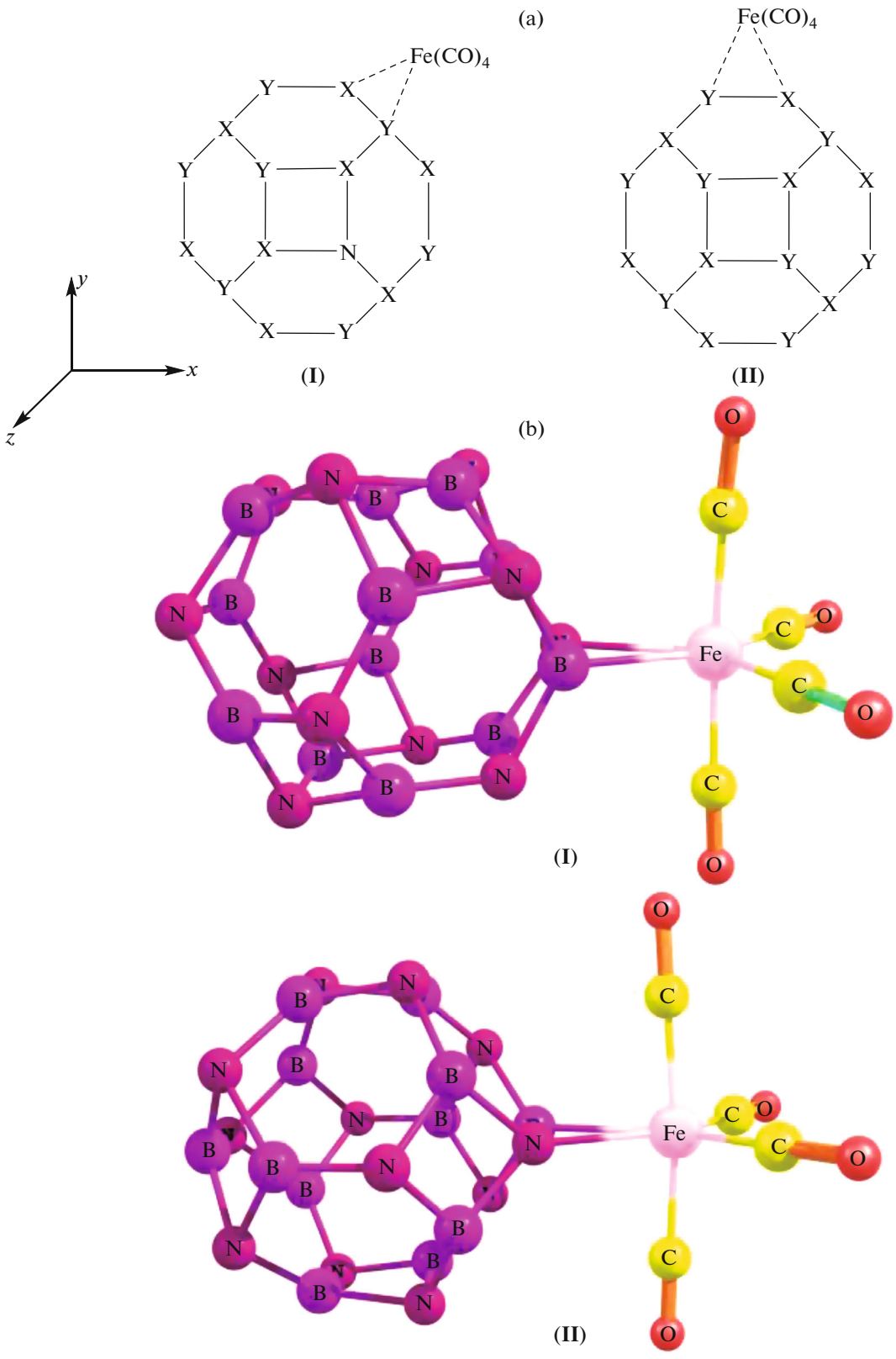

Fig. 1. (a) Front view and (b) 3D structures of two coordination modes of the $Fe(CO)_4$ fragment to $[X_{12}Y_{12}]$ (X = B or Al, Y = N or P) nano-cages.

Table 2. Fe–C, Fe–X, and Fe–Y bonding distances (in pm) of the $Fe(CO)_4[X_{12}Y_{12}]$ (X = B or Al, Y = N or P) complexes

Molecule	r(Fe–CO_{eq})		r(Fe–CO_{ax})	r(Fe–X)	r(Fe–Y)
	trans to X	*trans* to Y			
BN-**I**	180.21	175.92	181.67	214.22	207.36
BN-**II**	181.39	176.65	181.19	211.39	204.29
AlN-**I**	180.25	176.76	179.68	244.62	211.57
AlN-**II**	180.08	177.07	179.66	239.90	210.19
BP-**I**	179.50	176.70	181.59	219.38	230.85
BP-**II**	179.82	176.68	180.96	221.16	228.23
AlP-**I**	179.40	175.87	180.42	245.78	240.11
AlP-**II**	179.88	176.00	180.43	244.90	237.26

Table 3. Energy decomposition analysis (EDA) and thermochemical analysis results (kcal/mol) of interaction of $Fe(CO)_4$ fragment to $[X_{12}Y_{12}]$ (X = B or Al, Y = N or P) nano-cages

Molecule	ΔE_{int}	ΔE_{polar}	ΔE_{steric}	ΔG	ΔH
BN-**I**	–50.97	–90.50	39.52	15.27	14.56
BN-**II**	–57.86	–99.84	41.98	7.66	7.11
AlN-**I**	–66.55	–91.56	25.01	–18.49	–18.98
AlN-**II**	–69.37	–95.10	25.73	–26.36	–27.21
BP-**I**	–61.03	–115.63	54.60	–3.78	–5.53
BP-**II**	–61.94	–117.90	55.97	–6.62	–7.95
AlP-**I**	–65.41	–109.96	44.55	–18.09	–19.59
AlP-**II**	–64.28	–111.22	46.94	–20.23	–20.99

I than isomer **II**. On the other hand, Fe–Co_{ax} bond distances are longer than average of Fe–CO_{eq} bond distances. The Fe–CO bond distance is 178.1 pm in free $Fe(CO)_4$. It can be found, Fe–CO_{ax} bond distances are longer than free $Fe(CO)_4$. Therefore, electron density of Fe–CO_{ax} is smaller than Fe–CO_{ax} fragment. On the other hand, Fe–CO bonds are longer in *trans* position to X than *cis* position to Y.

Energy Decomposition Analysis (EDA)

Energy decomposition analysis (EDA) was useful to explain interactions of $Fe(CO)_4$ fragment to $[X_{12}Y_{12}]$ (X = B or Al, Y = N or P) nano-cages. EDA results calculations are listed in Table 3. It can be observed, interactions are stronger in $Fe(CO)_4\cdots[B_{12}P_{12}]$ complexes than $Fe(CO)_4\cdots[B_{12}N_{12}]$ complexes. On the other hand, it can be found stronger interactions for $Fe(CO)_4\cdots[Al_{12}N_{12}]$ complexes than $Fe(CO)_4\cdots[Al_{12}P_{12}]$ complexes. EDA consequences specify the most negative ΔE_{int} value in the $Fe(CO)_4\cdots[Al_{12}N_{12}]$ molecule.

The negative polarization energy values stabilize these molecules. The computed most negative ΔE_{polar} values is observed for $Fe(CO)_4\cdots[B_{12}P_{12}]$ molecule. Moreover, positive steric values energy destabilized these molecules. The calculated most positive ΔE_{steric} values is revealed for $Fe(CO)_4\cdots[B_{12}P_{12}]$ molecule.

Dipole Moment

Dipole moment values of the $Fe(CO)_4[X_{12}Y_{12}]$ (X = B or Al, Y = N or P) complexes are calculated (Table 1). The calculated dipole moment values show that polarity of the studied complexes depend on the nano-cage character. It can be deduced, this property decreases as: $[B_{12}P_12]$ > $[Al_{12}P_{12}]$ > $[B_{12}N_{12}]$ > $[Al_{12}N_{12}]$. On the other hand, polarity of isomer **II** is larger than isomer **I** in the presence of $[B_{12}N_{12}]$, $[Al_{12}N_{12}]$, and $[Al_{12}P_{12}]$ nano-cages. This property is larger for isomer **I** than isomer **II** in the presence of $[B_{12}P_{12}]$ nano-cage. The most polarity is attributed to isomer **II** of $Fe(CO)_4[B_{12}P_{12}]$ complex.

Polarizability

Isotropic polarizability values of the $Fe(CO)_4[X_{12}Y_{12}]$ (X = B or Al, Y = N or P) complexes are calculated (Table 1). Isotropic polarizability $\langle\alpha_{iso}\rangle$ was calculated using following equation and considering only diagonal elements:

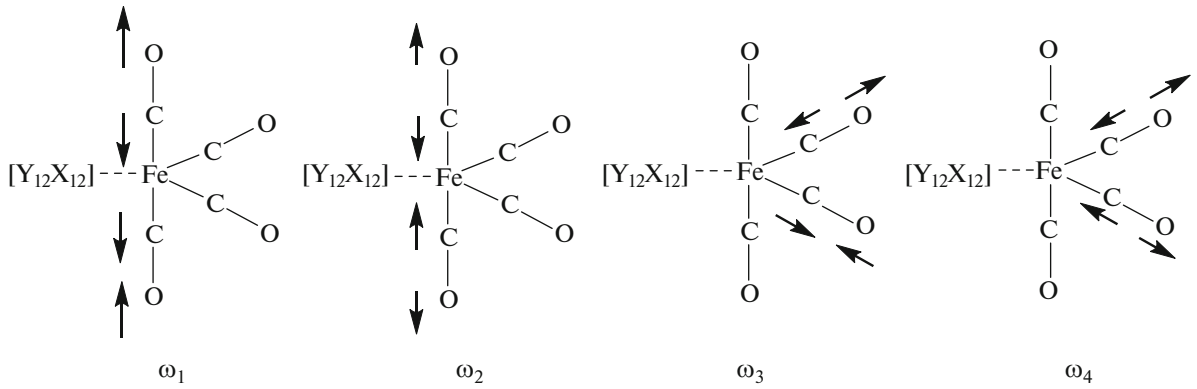

Fig. 2. Stretching vibrational modes of carbonyl ligands in the investigated complexes.

$$\alpha_{iso} = \frac{\alpha_{xx} + \alpha_{yy} + \alpha_{zz}}{3}.$$

It can be observed these values show that polarity of the studied complexes depend on the nano-cage character. This property decreases as: $[Al_{12}P_{12}] > [B_{12}P_{12}] > [Al_{12}N_{12}] > [B_{12}N_{12}]$. It can be observed, the most polarizability is attributed to $Fe(CO)_4[Al_{12}P_{12}]$ complexes. Least electronegativity and largest size values of Al and P than other atoms cause the electron could is most easily distorted in $Fe(CO)_4[Al_{12}P_{12}]$ complexes.

Vibrational Analysis

Stretching vibrational modes of carbonyl ligands are indicated in Fig. 2. Frequencies values of these vibrations (ω) are listed in Table 4. It can be found that the values of ω_1 and ω_2 (symmetric and asymmetric vibrational frequencies values of CO_{axial} bonds) are larger than ω_3 and ω_4 values (those values of $CO_{equatorial}$ bonds). On the other hand, asymmetric stretching vibrational frequencies (ω_1 and ω_3) are smaller than symmetric vibrational frequencies (ω_2 and ω_4).

Thermochemical Analysis

Thermodynamics parameters of the interactions of $Fe(CO)_4$ fragment and $[X_{12}Y_{12}]$ nano-cages are calculated by the following reaction equation:

$$Fe_2(CO)_9 + 2[X_{12}Y_{12}] \rightarrow$$
$$\rightarrow [X_{12}Y_{12}]\cdots Fe(CO)_4 + 2CO; \quad \Delta X = G, H.$$

Free $Fe(CO)_4$ fragment is not stable, therefore $Fe_2(CO)_9$ complex is considered as a reference level for illustration of thermodynamics of the $[X_{12}Y_{12}]\cdots Fe(CO)_4$ formations. Free energy change (ΔG) and enthalpy change (ΔH) values of these reaction are gathered in Table 3 at 298 K and 1 atm. It can be concluded, these reactions are spontaneous and exothermic in the presence of $[Al_{12}N_{12}]$, $[B_{12}P_{12}]$, and $[Al_{12}P_{12}]$ nano-cages.

Table 4. Vibrational frequencies values of the stretching vibrational modes of Fe-CO bonds vibrations in the $Fe(CO)_4[X_{12}Y_{12}]$ (X = B or Al, Y = N or P) complexes (ω, cm^{-1}). Scale factor 0.9567 is considered from Computational Chemistry Comparison and Benchmark DataBase (https://cccbdb.nist.gov/vsf2x.asp)

Molecule	ω_1	ω_2	ω_3	ω_4
BN-**I**	2028.55	2053.15	2062.01	2119.52
BN-**II**	2036.89	2058.06	2061.27	2118.21
AlN-**I**	2006.91	2026.76	2038.75	2092.52
AlN-**II**	2007.78	2028.52	2037.11	2092.25
BP-**I**	2041.23	2058.64	2065.66	2113.23
BP-**II**	2042.65	2059.78	2061.21	2109.33
AlP-**I**	2029.88	2046.92	2056.03	2101.10
AlP-**II**	2034.80	2047.77	2058.26	2101.52

Table 5. Frontier orbital energy, hardness (η), and chemical potential (μ) of $Fe(CO)_4$ and $[X_{12}Y_{12}]$ (X = B or Al, Y = N or P) nano-cages (eV)

Molecule	*E*(HOMO)	*E*(LUMO)	η	μ
$[B_{12}N_{12}]$	−8.23	−0.83	3.70	−4.53
$[Al_{12}N_{12}]$	−6.84	−2.31	2.27	−4.57
$[B_{12}P_{12}]$	−7.27	−3.19	2.04	−5.23
$[Al_{12}P_{12}]$	−7.07	−3.55	1.76	−5.31
$Fe(CO)_4$	−6.75	−3.17	1.79	−4.96

In addition, ΔG values show that isomer **II** formation reactions are more spontaneous than isomer **I**. However, the reactions are non-spontaneous and endothermic in the presence $[B_{12}N_{12}]$.

Electrophilicity-Based Charge Transfer (ECT)

The electrophilicity-based charge transfer (ECT) values of $Fe(CO)_4[X_{12}Y_{12}]$ (X = B or Al, Y = N or P) isomers are evaluated. The difference between ΔN_{max} values of interacting molecules is defined as ECT [61]:

$$\mathrm{ECT} = \Delta N_{\max}(\mathrm{Fe(CO)_4}) - \Delta N_{\max}(\mathrm{X_{12}Y_{12}}),$$

where ΔN_{max} is defined as:

$$(\Delta N_{\max})_i = \frac{\mu_i}{\eta_i}.$$

In this equation, η and μ are global hardness and chemical potential, respectively. They are provided on the basis of Koopman's theorem [62] and known as global reactivity descriptors [63–66]. These values for $Fe(CO)_4$, $[X_{12}Y_{12}]$ molecules are computed by the subsequent equations and results are mentioned in Table 5.

$$\eta = \frac{E(\mathrm{LUMO}) - E(\mathrm{HOMO})}{2},$$

$$\mu = \frac{E(\mathrm{HOMO}) + E(\mathrm{LUMO})}{2}.$$

The calculated ΔN_{max} value are −1.54, −0.75, −0.20, and 0.25 for interaction of $Fe(CO)_4$ with $[B_{12}N_{12}]$, $[Al_{12}N_{12}]$, $[B_{12}P_{12}]$, and $[Al_{12}P_{12}]$, respectively. The positive value of ECT reveals charge flow from $[Al_{12}P_{12}]$ to $Fe(CO)_4$. On the other hand, the negative values of ECT show charge flow from $Fe(CO)_4$ to $[B_{12}N_{12}]$, $[Al_{12}N_{12}]$, and $[B_{12}P_{12}]$.

Hyperpolarizability

The first hyperpolarizabilities values of the $Fe(CO)_4[X_{12}Y_{12}]$ (X = B or Al, Y = N or P) complexes are calculated. The β_{tot}, β_x, β_y, and β_z values of these complexes are presented in Table 6. The calculated β_{tot} values show that NLO properties of the studied complexes depend on the nano-cage character. It can be deduced; this property increases as: $[B_{12}N_{12}] < [Al_{12}N_{12}] < [B_{12}P_{12}] < [Al_{12}P_{12}]$. On the other hand, NLO property of isomer **I** is larger than isomer **II** in the presence of $[B_{12}N_{12}]$, $[Al_{12}N_{12}]$, and $[B_{12}P_{12}]$ nano-cages. This property is larger for isomer **II** than isomer **I** in the presence of $[Al_{12}P_{12}]$ nano-cage. The most activity of NLO is attributed to isomer **II** of $Fe(CO)_4[Al_{12}P_{12}]$ complex.

QTAIM

Results of QTAIM computations at the bond critical points (BCP) of Fe–C, Fe–X, and Fe–Y bonds of the $Fe(CO)_4[X_{12}Y_{12}]$ (X = B or Al, Y = N or P) complexes are listed in Table 7. Larger ρ_{BCP}(Fe–X) and ρ_{BCP}(Fe–X) values are well-matched with longer Fe–X and Fe–Y (Table 2). There is good linear correlation between ρ_{BCP}(Fe–X) and *r*(Fe–X) values:

$$\rho_{\mathrm{BCP}} = -0.0009r(\mathrm{Fe} - \mathrm{X}) + 0.263; \quad R^2 = 0.9936.$$

Maximum electron density in bond critical points is belonged to Fe–It can be seen, $\rho_{BCP}(Fe–C_{ax})$ values are smaller than $\rho_{BCP}(Fe–C_{eq})$ in the studied complexes. These results are compatible with longer Fe–C_{ax} bonds than Fe–C_{eq} bonds.

Positive Laplacian of electron density ($\nabla^2\rho$) values are compatible with closed–shell interactions for the Fe–C, Fe–X and Fe–Y bonds.

The negative total electron energy density (*H*) values are considered as an indicator of covalency. There is the following equation between *H* and its components:

$$H = G + V.$$

In this equation, *V* and *G* are virial energy density and Lagrangian kinetic energy, respectively. The positive $\nabla^2\rho$ values and negative *H* values of Fe–C, Fe–X and Fe–Y bonds are compatible with similar systems [67, 68]. These values are compatible with a combina-

Table 6. Components and total first hyperpolarizability values (esu) of the $Fe(CO)_4[X_{12}Y_{12}]$ (X = B or Al, Y = N or P) complexes

	BN-**I**	BN-**II**	AlN-**I**	AlN-**II**	BP-**I**	BP-**II**	AlP-**I**	AlP-**II**
β_{xxx}	201.48	−4.10	392.16	−225.09	800.25	−790.28	1391.27	−1440.26
β_{xxy}	−8.95	0.03	−30.49	−7.06	−47.00	−2.15	−69.28	−3.14
β_{xyy}	32.01	46.71	312.88	−315.11	300.64	−279.02	418.48	−434.21
β_{yyy}	16.55	−0.09	17.84	0.04	6.59	0.00	−23.22	−0.01
β_{xxz}	−25.11	−24.23	124.10	−109.33	−131.20	152.61	−63.98	126.79
β_{xyz}	18.49	−0.08	6.04	−3.93	24.24	−1.01	−0.65	1.01
β_{yyz}	−12.78	0.48	25.27	−22.07	−44.98	73.06	−40.36	73.16
β_{xzz}	−115.78	−138.82	195.94	−145.04	149.27	−142.93	228.95	−238.38
β_{yzz}	−4.45	0.51	20.20	−1.34	−58.36	1.53	−31.87	−0.16
β_{zzz}	−50.71	101.25	−112.25	152.46	−128.17	181.19	−119.69	181.83
β_{tot}	1.27×10^{-30}	1.07×10^{-30}	7.79×10^{-30}	5.92×10^{-30}	1.12×10^{-30}	1.11×10^{-30}	1.78×10^{-30}	1.86×10^{-30}
$10^{30}\beta_{tot}$	1.27	1.07	7.79	5.92	11.15	11.05	17.75	18.55

tion of the shared and closed–shell interactions for the Fe–L bonds.

$|V|/G$ ratio is useful for description of bond characterization. $|V(r)|/G(r) < 1$ and $V(r)|/G(r) > 2$ are characteristics of a typical ionic interaction and "classical" covalent interactions, respectively [69]. |V|/G rations of Fe–C, Fe–X and Fe–Y bonds are listed in Table 7. These values are between 1 and 2. Therefore, it can be observed mixture of the shared and closed–shell interactions for the Fe–L bonds.

Laplacian Bond Order (LBO)

Bond orders are valuable values to illustrate of the Fe–C, Fe–X, and Fe–Y bonds. An appropriated method of covalent bond is Laplacian bond order (LBO) [55]. In this method bond orders are computed in the basis of the Laplacian of electron density $\nabla^2\rho$ in fuzzy overlap space.

The calculated LBO values for Fe–C, Fe–X, and Fe–Y bonds in the studied complexes are listed in Table 8. These values show that, LBO values of Fe–C bond are close to 1, therefore, the Fe–C bonds are the covalent single bond. On the other hand, LBO values of Fe–X and Fe–Y bonds are smaller than 1 reveal that the weaker interactions in compared to the classic covalent single bond. There are good linear correlations between average of LBO and bond distances values of Fe–X and Fe–Y bonds as:

$$Fe(CO)_4 \cdots [X_{12}N_{12}](X = B \text{ and } Al): \langle LBO \rangle = -239.16\langle r \rangle + 241.62; \quad R^2 = 0.9949;$$

$$Fe(CO)_4 \cdots [X_{12}P_{12}](X = B \text{ and } Al): \langle LBO \rangle = -195.65\langle r \rangle + 271.76; \quad R^2 = 0.9502.$$

In addition, LBO values of Fe–CO bonds are smaller in *trans* position to X than *cis* position to Y. This result explains longer Fe–CO bonds are in *trans* position to X than *cis* position to Y.

Independent Gradient Model (IGM)

Independent Gradient Model (IGM) is a significance tool for illustration of interfragment and intrafragment interactions [56, 57]. The provided isosurface graphs of the studied systems are presented in Fig. 3. The major van der Waals interaction region is exhibited as green isosurface for each of molecules.

CONCLUSIONS

In this work, electronic, structural, and optical properties of $Fe(CO)_4$ $[X_{12}Y_{12}]$ (X = B or Al, Y = N or P) complexes were investigated at the mPW1PW91/6-311G(d,p) level of theory. According to the computations, isomer **II** was more stable than isomer **I**. EDA consequences identified the most interaction in the $Fe(CO)_4\cdots[Al_{12}N_{12}]$ molecule. The positive value of ECT revealed charge flow from $[Al_{12}P_{12}]$ to $Fe(CO)_4$.

Table 7. QTAIM results at the bond critical points of Fe–C, Fe–X, and Fe–Y bonds of the $Fe(CO)_4[X_{12}Y_{12}]$ (X = B or Al, Y = N or P) complexes

Molecule	$Fe–CO_{eq}$		$Fe–CO_{ax}$	Fe–X	Fe–Y
	trans to X	*trans* to Y			
Electron density (ρ, e Å^{-3})					
BN-I	0.1635	0.1445	0.1351	0.0744	0.0765
BN-II	0.1409	0.1581	0.1377	0.0782	0.0804
AlN-I	0.1452	0.1536	0.1444	–	0.0696
AlN-II	0.1457	0.1521	0.1455	–	0.0727
BP-I	0.1469	0.1365	0.1359	0.0729	0.0739
BP-II	0.1458	0.1608	0.1381	0.0709	0.0766
AlP-I	0.1479	0.1630	0.0625	0.0484	0.0644
AlP-II	0.1462	0.1462	0.1405	0.0488	0.0665
Laplacian of electron density (∇^2ρ, e Å^{-5})					
BN-I	0.5074	0.5370	0.5561	0.0207	0.3444
BN-II	0.5292	0.5246	0.5422	0.0162	0.3713
AlN-I	0.5230	0.5642	0.5338	–	0.2728
AlN-II	0.5240	0.5687	0.5303	–	0.2807
BP-I	0.5344	0.5476	0.5426	0.0284	0.1268
BP-II	0.5352	0.5021	0.5460	0.0265	0.1307
AlP-I	0.5329	0.5126	0.1155	0.0249	0.0907
AlP-II	0.5315	0.5315	0.5417	0.0281	0.1002
Energy density (*E*, a.u.)					
BN-I	–0.0780	–0.0592	–0.0511	–0.0311	–0.0111
BN-II	–0.0555	–0.0727	–0.0536	–0.0342	–0.0125
AlN-I	–0.0592	–0.0687	–0.0595	–	–0.0098
AlN-II	–0.0595	–0.0670	–0.0605	–	–0.0109
BP-I	–0.0618	–0.0523	–0.0519	–0.0273	–0.0216
BP-II	–0.0604	–0.0751	–0.0538	–0.0263	–0.0236
AlP-I	–0.0621	–0.0776	–0.0231	–0.0211	–0.0183
AlP-II	–0.0604	–0.0604	–0.0559	–0.0213	–0.0191
Lagrangian kinetic energy (*G*, a.u.)					
BN-I	0.2048	0.1934	0.1901	0.0363	0.0972
BN-II	0.1877	0.2039	0.1891	0.0383	0.1053
AlN-I	0.1899	0.2097	0.1930	–	0.0780
AlN-II	0.1905	0.2092	0.1931	–	0.0811
BP-I	0.1954	0.1892	0.1876	0.0344	0.0533
BP-II	0.1942	0.2006	0.1903	0.0329	0.0563
AlP-I	0.1954	0.2057	0.0520	0.0273	0.0410
AlP-II	0.1933	0.1933	0.1913	0.0283	0.0441

Table 7. (Contd.)

Potential energy density (V, a.u.)					
Molecule	Fe–CO_{eq}		Fe–CO_{ax}	Fe–X	Fe–Y
	trans to X	*trans* to Y			
BN-**I**	–0.2828	–0.2526	–0.2411	–0.0674	–0.1082
BN-**II**	–0.2432	–0.2766	–0.2427	–0.0725	–0.1177
AlN-**I**	–0.2491	–0.2784	–0.2525	–	–0.0877
AlN-**II**	–0.2501	–0.2762	–0.2537	–	–0.0920
BP-**I**	–0.2571	–0.2416	–0.2395	–0.0617	–0.0749
BP-**II**	–0.2546	–0.2757	–0.2441	–0.0593	–0.0799
AlP-**I**	–0.2575	–0.2833	–0.0751	–0.0484	–0.0593
AlP-**II**	–0.2537	–0.2537	–0.2472	–0.0495	–0.0632
$\|V\|/G$					
Molecule	Fe–CO_{eq}		Fe–CO_{ax}	Fe–X	Fe–Y
	trans to X	*trans* to Y			
BN-**I**	1.38	1.31	1.27	1.86	1.11
BN-**II**	1.30	1.36	1.28	1.89	1.12
AlN-**I**	1.31	1.33	1.31		1.12
AlN-**II**	1.31	1.32	1.31		1.13
BP-**I**	1.32	1.28	1.28	1.79	1.41
BP-**II**	1.31	1.37	1.28	1.80	1.42
AlP-**I**	1.32	1.38	1.44	1.77	1.45
AlP-**II**	1.31	1.31	1.29	1.75	1.43

Table 8. Calculated LBO values for Fe–C, Fe–X, and Fe–Y bonds in the studied complexes

Molecule	Fe–CO_{eq}		Fe–CO_{ax}	Fe–X	Fe–Y
	trans to X	*trans* to Y			
BN-**I**	0.9640	1.0128	1.0234	0.1195	0.1359
BN-**II**	0.9535	1.033	1.0147	0.1294	0.1556
AlN-**I**	0.9851	1.0640	0.9977	0.0375	0.0826
AlN-**II**	0.9858	1.0620	0.9909	0.0408	0.0908
BP-**I**	0.9780	1.0028	1.0041	0.1820	0.3176
BP-**II**	0.9792	1.0013	1.0186	0.1335	0.3173
AlP-**I**	0.9847	1.0135	1.0166	0.0652	0.2388
AlP-**II**	0.9725	1.0199	1.0138	0.0603	0.2513

On the other hand, the negative values of ECT indicated charge flow from $Fe(CO)_4$ to $[B_{12}N_{12}]$, $[Al_{12}N_{12}]$, and $[B_{12}P_{12}]$. LBO values of Fe–C bond were close to 1 indicate that the Fe–C bonds were the covalent single bond. The negative H and positive $\nabla^2\rho$ values of Fe–C, Fe–X, and Fe–Y bonds revealed mixture of the shared and closed–shell interactions for the Fe–L bonds. On the other hand, LBO <1 values of Fe–X and Fe–Y bonds indicated the weaker interactions than the covalent single bond. As future outlook of this study, solvent effect on the calculated parameters can be useful. Dielectric constant dependency of

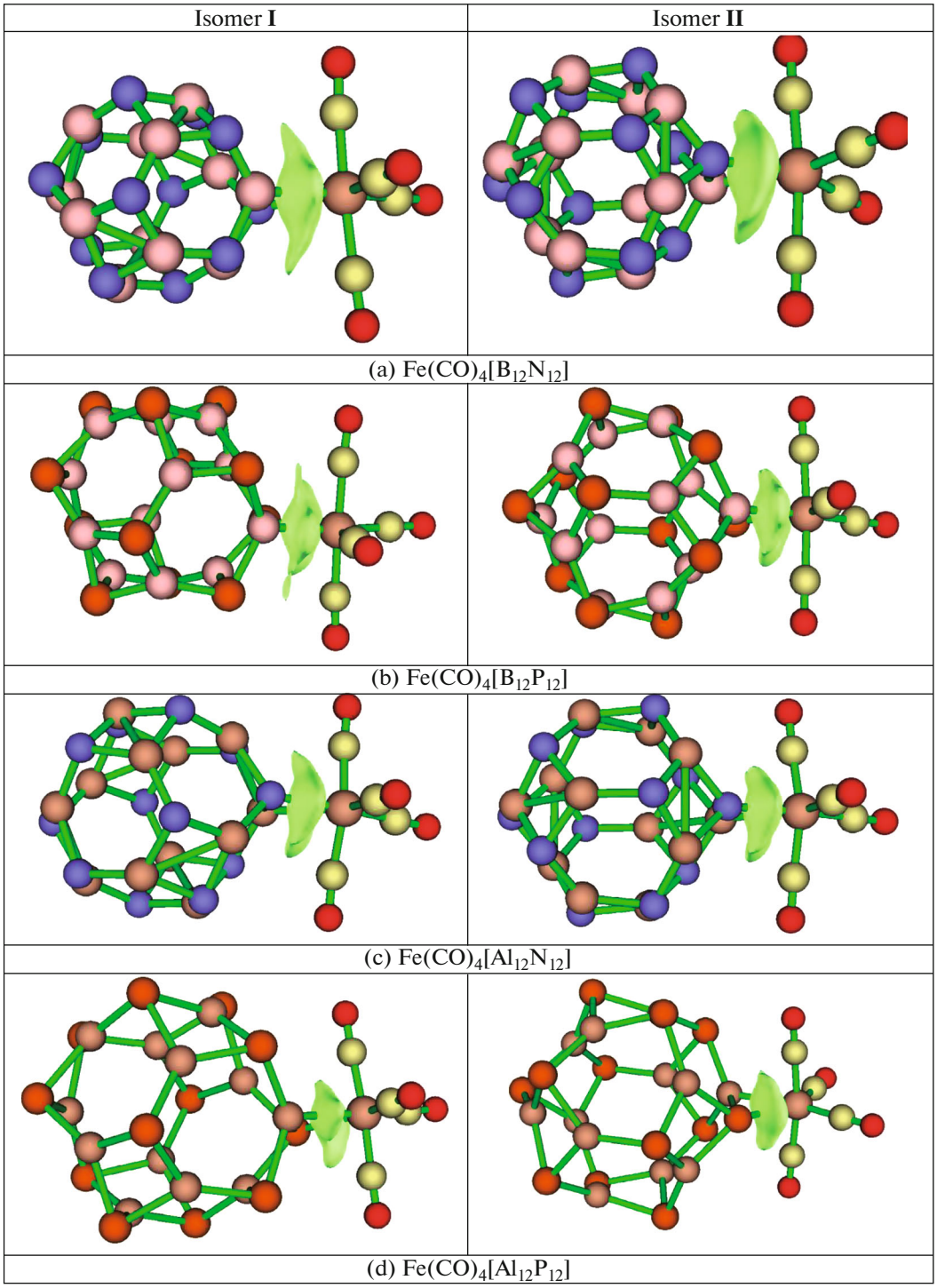

Fig. 3. IGM analysis results of the studied complexes.

the solvent on these parameters will give useful information.

CONFLICT OF INTEREST

The authors declare that they have no conflicts of interest.

REFERENCES

1. L. S. Cunden and R. G. Linck, Inorg. Chem. **50**, 4428 (2011). https://doi.org/10.1021/ic200009w
2. Y. Chen, M. Hartmann, and G. Frenking, Z. Anorg. Allg. Chem. **627**, 985 (2001).

https://doi.org/10.1002/1521-3749(200105)627:5<985::AID-ZAAC985>3.0.CO;2-%23

3. T. A. Albright, J. K. Burdett, and M.-H. Whangbo, *Orbital Interactions in Chemistry*, 2nd ed. (John Wiley and Sons, Hoboken, NJ, 2013).
4. C. L. B. Macdonald,A. H. Cowley, J. Am. Chem. Soc. **121**, 12113 (1999). https://doi.org/10.1021/ja992573l
5. T. H. Cymbaluk and R. D. Ernst, Inorg. Chem. **19**, 2381 (1980). https://doi.org/10.1021/ic50210a041
6. J. Su, X.-W. Li, R. C. Crittendon, C. F. Campana, and G. H. Robinson, Organometallics **16**, 4511 (1997). https://doi.org/10.1021/om970530c
7. A. H. Cowley, V. Lomeli, and A. Voigt, J. Am. Chem. Soc. **120**, 6401 (1998). https://doi.org/10.1021/ja9806433
8. P. Jutzi, B. Neumann, G. Reumann, and H.-G. Stammler, Organometallics **17**, 1305 (1998). https://doi.org/10.1021/om970913a
9. G. Spessard and G. Miessler, *Organometallic Chemistry* (Oxford University Press, New York, 2009).
10. N. K. Neumolotov, N. A. Selivanov, A. Y. Bykov, et al., Russ. J. Inorg. Chem. **67**, 1583 (2022). https://doi.org/10.1134/S0036023622600861
11. I. N. Klyukin, A. S. Novikov, A. P. Zhdanov, et al., Russ. J. Inorg. Chem. **64**, 1825 (2019). https://doi.org/10.1134/S0036023619140031
12. A. V. Nelyubin, N. A. Selivanov, A. Y. Bykov, et al., Russ. J. Inorg. Chem. **65**, 795 (2020). https://doi.org/10.1134/S0036023620060133
13. J. A. Talla, K. Al-Khaza'leh, and N. Omar, Russ. J. Inorg. Chem. **67**, 1025 (2022). https://doi.org/10.1134/S0036023622070178
14. M. Monajjemi, Russ. J. Inorg. Chem. **66**, 2091 (2021). https://doi.org/10.1134/S0036023621140035
15. V. V. Avdeeva, E. A. Malinina, and N. T. Kuznetsov, Coord. Chem. Rev. **469**, 214636 (2022). https://doi.org/10.1016/j.ccr.2022.214636
16. V. V. Avdeeva, E. A. Malinina, N. T. Kuznetsov, Russ. J. Inorg. Chem. **65**, 335 (2020). https://doi.org/10.1134/S003602362003002X
17. V. V. Avdeeva, T. M. Garaev, E. A. Malinina, et al., Russ. J. Inorg. Chem. **67**, 28 (2022). https://doi.org/10.1134/S0036023622010028
18. D. L. Strout, J. Phys. Chem. A **104**, 3364 (2000). https://doi.org/10.1021/jp994129a
19. R. Wang, D. Zhang, and C. Liu, Chem. Phys. Lett. **411**, 333 (2005). https://doi.org/10.1016/j.cplett.2005.06.055
20. B. Bertolus, F. Finocchi, and P. Millie, J. Chem. Phys. **120**, 4333 (2004). https://doi.org/10.1063/1.1636717
21. C.-C. Fu, M. Weissmann, M. Machado, and P. Ordejón, Phys. Rev. B **63**, 85411 (2001). https://doi.org/10.1103/PhysRevB.63.085411
22. M. Bilge, J. Struct. Chem. **59**, 1271 (2018). . https://doi.org/10.1134/S0022476618060045
23. A. K. Kandalam, M. A. Blanco, and R. Pandey, J. Phys. Chem. B **105**, 6080 (2001). https://doi.org/10.1021/jp004404p
24. E. S. E. Tahmasebi and Z. Biglari, Appl. Surf. Sci. **363**, 197 (2016). https://doi.org/10.1016/j.apsusc.2015.12.001
25. Q. W. F. Zhang, X. Wang, N. Liu, J. Yang, Y. Hu, L. Yu, Z. Hu, and J. Zhu, J. Phys. Chem. C **113**, 4053 (2009). https://doi.org/10.1021/jp811484r
26. M. Shabani, R. Ghiasi, K. Zarea, and R. Fazaeli, Russ. J. Inorg. Chem. **65**, 1726 (2020). https://doi.org/10.1134/S0036023620110169
27. L. Palomino-Asencio, E. García-Hernándeza, M. Salazar-Villanueva, and E. Chigo-Anota, Physica E **126**, 114456 (2021). https://doi.org/10.1016/j.physe.2020.114456
28. R. Pino-Rios, E. Chigo-Anota, E. Shakerzadeh, and G. Cárdenas-Jirón, Physica E **115**, 113697 (2020). https://doi.org/10.1016/j.physe.2019.113697
29. A. Escobedo-Morales, L. Tepech-Carrillo, A. Bautista-Hernández, J. H. Camacho-García, D. Cortes-Arriagada, and E. Chigo-Anota, Sci. Rep. **9**, 16521 (2019). doi 1-11 . https://doi.org/10.1038/s41598-019-52981-1
30. K. Ayub, J. Mol. Liq. **244**, 124 (2017). https://doi.org/10.1016/j.molliq.2017.08.118
31. K. Ayub, Int. J. Hydrogen Energy **42**, 11439 (2017). https://doi.org/10.1016/j.ijhydene.2017.02.202
32. O. P. Charkin and N. M. Klimenko, Russ. J. Inorg. Chem. **63**, 479 (2018). https://doi.org/10.1134/S0036023618040058
33. O. P. Charkin and N. M. Klimenko, Russ. J. Inorg. Chem. **64**, 770 (2019). https://doi.org/10.1134/S0036023619060196
34. A. K. Srivastava, S. K. Pandey, and N. Misra, J. Nanostruct. Chem. **5**, 103 (2016). https://doi.org/10.1007/s40097-015-0184-8
35. J. Beheshtian, Z. Bagheri, M. Kamfiroozi, and A. Ahmadi, J. Mol. Model. . **18**, 2653 (2012). https://doi.org/10.1007/s00894-011-1286-y
36. A. S. Rad and K. Ayub, J. Alloys Compd. **672**, 161 (2016). https://doi.org/10.1016/j.jallcom.2016.02.139
37. S.Hussain, S. A. S. Chatha, A. I. Hussain, R. Hussain, M. Y. Mehboob, T. Gulzar, A. Mansha, N. Shahzad, and K. Ayub, ACS Omega **5**, 15547 (2020). https://doi.org/10.1021/acsomega.0c01686
38. F. Ullah, S. Irshad, S. Khana, M. A. Hashmi, R. Ludwigc, T. Mahmood, and K. Ayub, J. Phys. Chem. Solids **151**, 109914 (2021). https://doi.org/10.1016/j.jpcs.2020.109914
39. S. Irshad, F. Ullah, S. Khan, R. Ludwigb, T. Mahmood, and K. Ayub, Optics Laser Technol. **134**, 106570 (2021). https://doi.org/10.1016/j.optlastec.2020.106570
40. F. Ullah, N. Kosar, A. A. Maria, T. Mahmood, and K. Ayub, Physica E **118**, 113906 (2020). https://doi.org/10.1016/j.physe.2019.113906
41. S.Onsori and E. Alipour, J. Mol. Graph. Model. **79**, 223 (2018). https://doi.org/10.1016/j.jmgm.2017.12.007
42. M. Shabani, R. Ghiasi, K. Zare, and R. Fazaeli, Main Group Chem. **20**, 345 (2021). https://doi.org/10.3233/MGC-210051

43. M. Rezaei-Sameti and M. Jafari, Chem. Methodol. **4**, 494 (2020). https://doi.org/10.33945/SAMI/CHEMM.2020.4.10
44. M. Abbasi, E. Nemati-Kande, and M. D. Mohammadi, Comput. Theor. Chem. **1132**, 1 (2018). https://doi.org/10.1016/j.comptc.2018.04.003
45. R. H. Herber, E. Bauminger, and I. Felner, J. Chem. Phys. **104**, 7 (1996). https://doi.org/10.1063/1.470869
46. M. J. Frisch, G. W. Trucks, H. B. Schlegel, et al., Gaussian 09, Revision A.02 (Gaussian, Inc., Wallingford CT, 2009).
47. P. C. Hariharan and J. A. Pople, Theor. Chim. Acta **28**, 213 (1973). https://doi.org/10.1007/BF00533485
48. P. C. Hariharan and J. A. Pople, Mol. Phys. **27**, 209 (1974). https://doi.org/10.1080/00268977400100171
49. C. Adamo and V. Barone, J. Chem. Phys. **108**, 664 (1998). https://doi.org/10.1063/1.475428
50. R. C. Dunbar, J. Phys. Chem. A **106**, 7328 (2002). https://doi.org/10.1021/jp013588k
51. M. Porembski and J. C. Weisshaar, J. Phys. Chem. A **105**, 6655 (2001). https://doi.org/10.1021/jp010646t
52. M. Porembski and J. C. Weisshaar, J. Phys. Chem. A **105**, 4851 (2001). https://doi.org/10.1021/jp010219f
53. Y. Zhang, Z. Guo, and X.-Z. You, J. Am. Chem. Soc. **123**, 9378 (2001). https://doi.org/10.1021/ja0023938
54. T. Lu and F. Chen, J. Mol. Graph. Model. **38**, 314 (2012). https://doi.org/10.1016/j.jmgm.2012.07.004
55. T. Lu and F. Chen, J. Phys. Chem. A **117**, 3100 (2013). https://doi.org/10.1021/jp4010345
56. C. Lefebvre, G. Rubez, H. Khartabil, J.-C. Boisson, J. Contreras-Garcia, and E. Hénon, Phys. Chem. Chem. Phys. **19**, 17928 (2017). https://doi.org/10.1039/C7CP02110K
57. C. Lefebvre, H. Khartabil, J.-C. Boisson, J. Contreras-García, J.-P. Piquemal, and E. Hénon, ChemPhys Chem **19**, 724 (2018).
58. T. Lu and F. Chen, J. Mol. Graph. Model. **38**, 314 (2012). https://doi.org/10.1016/j.jmgm.2012.07.004
59. T. Lu and F. Chen, J. Comp. Chem. **33**, 580 (2012). https://doi.org/10.1002/jcc.22885
60. D. A. Keleiman, Phys. Rev. **126**, 1977 (1962). https://doi.org/10.1103/PhysRev.126.1977
61. J. Padmanabhan, R. Parthasarathi, V. Subramanian, and P. K. Chattaraj, J. Phys. Chem. A **111**, 1358 (2007). https://doi.org/10.1021/jp0649549
62. R. G. Parr and W. Yang, *Density Functional Theory of Atoms and Molecules* (Oxford University Press, Oxford, New York, 1989).
63. P. Geerlings, F. De Proft, and W. Langenaeker, Chem. Rev. **103**, 1793 (2003). https://doi.org/10.1021/cr990029p
64. R. G. Parr and R. G. Pearson, J. Am. Chem. Soc. **105**, 7512 (1983). https://doi.org/10.1021/ja00364a005
65. R. G. Parr, L. v. Szentpály, and S. Liu, J. Am. Chem. Soc. **121**, (1999). https://doi.org/10.1021/ja983494x
66. L. A. Flippin, D. W. Gallagher, and K. Jalali-Araghi, J. Org. Chem. **54**, (1989). https://doi.org/10.1021/jo00267a035
67. M. Palusiak, J. Organomet. Chem. **692**, 3866 (2005). https://doi.org/10.1016/j.jorganchem.2007.05.029
68. P. Macchi and A. Sironi, Coord. Chem. Rev. **239**, 383 (2003). https://doi.org/10.1016/S0010-8545(02)00252-7
69. I. Cukrowski, J. H. d. Lange, and M. Mitoraj, J. Phys. Chem. A **118**, 623 (2014). https://doi.org/10.1021/jp410744x